Construction and Building Materials 329 (2022) 127028

Contents lists available at ScienceDirect

Construction and Building Materials

journal homepage: www.elsevier.com/locate/conbuildmat

Durability assessment of GFRP rebars in marine environments

Alvaro Ruiz Emparanza [a,*], Raphael Kampmann [b], Francisco De Caso [a], Carlos Morales [a], Antonio Nanni [a]

[a] University of Miami, 1251 Memorial Drive, Coral Gables, 33146, FL, USA
[b] FAMU-FSU College of Engineering, 2525 Pottsdamer Street, Tallahassee, 32310, FL, USA

ARTICLE INFO

Keywords:
Composite FRP rebar
Durability
Service life
Marine structures
Reinforced concrete

ABSTRACT

Technologies developed over the last two decades have facilitated the use of glass fiber reinforced polymer (GFRP) bars as internal reinforcement for concrete structures, specially in coastal environments, mainly due to their corrosion resistance. To-date, most durability studies have focused on a single mechanical parameter (tensile strength) and a single aging environment (exposure to high alkalinity). However, knowledge gaps exists in understanding how other mechanical parameters and relevant conditioning environments may affect the durability of GFRP bars. To this end, this study assesses the durability for different physio-mechanical properties of GFRP rebars, post exposure to accelerated conditioning in seawater.

Six different GFRP rebar types were submerged in seawater tanks, at various temperatures (23 °C, 40 °C and 60 °C) for different time periods (60, 120, 210 and 365 days). In total six different physio-mechanical properties were assessed, including: tensile strength, E-modulus, transverse and horizontal shear strength, micro-structural composition and lastly, bond strength. It was inferred that rebars with high moisture absorption resulted in poor durability, in that it affected mainly the tensile strength. Based on the Arrhenius model, at 23 °C all the rebars that met the acceptance criteria by ASTM D7957 are expected to retain 85 % of the tensile strength capacity.

1. Introduction

In the last three decades, the use of glass fiber reinforced polymer (GFRP) rebars has increased worldwide, and is now recognized to be a viable alternative to steel for reinforced concrete structures [1]. These composite materials are made from longitudinally aligned fibers, embedded in a resin matrix. The fibers are responsible for carrying the load while the resin binds the fibers together, which guarantees load transfer among the individual fibers and protects them from degradation [2]. These rebars are globally produced, using 'pultrusion' processes, and offer various advantages compared to steel rebars: the main benefit is the extended durability but other advantages include high tensile strength (2–3 times higher than steel), lightweight (1/4 of the weight of the steel), transparency to magnetic fields and radar frequencies, as well as the lack of electric and thermal conduction [2].

Among the listed properties, an extended durability (and therefore, and extended service life of the built infrastructure), is assumed to be the key benefit of this alternative reinforcing technology used in concrete structures. To evaluate the durability of materials such as GFRP rebars, accelerated test protocols have been developed to assess in a relative short period of time the long term behavior of GFRP bars by exposing the material to a harsher environment than the one that would be exposed to service conditions. To this end, elevated temperatures are used as a mechanism to accelerate the aging [3]. In addition, different aging solutions are frequently used to simulate the different conditions to which the rebars are exposed in real life. Results from the accelerated aging experiments can then be used to predict the service life of the rebar for the duration of its service life.

Many research projects exist, that have evaluated the durability of GFRP rebars exposed to different solution (and different temperatures), such as high pH (simulating the high alkalinity of the pore solution of concrete), tap water (i.e.; to evaluate the effect of moisture in submerged applications), simulated seawater (conditions experienced in coastal regions), etc. [4–20]. Various of these studies and the characteristics of the accelerated conditioning protocol adopted by each of them are summarized in Table 1.

It can be inferred that the deterioration of the tensile strength was the main focus of past studies, though a few projects studied the degradation of the horizontal/transverse shear strength and the bond-to-concrete strength. Recently, Khatib et al. [15] studied the durability of GFRP rebars embedded in seawater-mixed concrete at 60 °C for up to two years, evaluating the retention of tensile properties (strength and modulus of elasticity), transverse/horizontal shear strength and bond

* Corresponding author.
E-mail address: alvaro.ruiz@miami.edu (A. Ruiz Emparanza).

https://doi.org/10.1016/j.conbuildmat.2022.127028
Received 2 November 2021; Received in revised form 4 February 2022; Accepted 1 March 2022

Table 1
Exposure condition and evaluated mechanical properties for various studies.

Research study	FRP type[a]	Analyzed mechanical properties	Accelerated aging		
			Conditioning	Duration d	Temperature °C
Khatib et al. [15]	GFRP	Tensile, transverse/horizontal shear & bond	Seawater-mixed concrete	≤730	60
Manalo et al. [20]	GFRP	Horizontal shear	Simulated seawater, tap water & alkaline sol.	≤112	23, 60, 80
Wang et al. [17]	B, C, & GFRP	Horizontal shear	Simulated seawater & sea sand concrete	≤84	25, 40, 55
Wang et al. [8]	B, & GFRP	Tensile	Simulated seawater & sea sand concrete	≤63	23, 40, 48, 55
Yan and Lin [18]	GFRP	Bond	Saline solutions	≤60	50, 70
Benmokrane et al. [10]	GFRP	Tensile, flexure & horizontal shear	Alkaline solution	≤90	60
Benmokrane et al. [19]	GFRP	Transverse/horizontal shear & flexure	Alkaline solution	≤210	60
Dong et al. [5]	B, & GFRP	Bond	Simulated seawater	≤240	25, 40, 55
Benmokrane et al. [9]	B, & GFRP	Transverse/horizontal shear & flexure	Alkaline solution	≤210	60
Robert and Benmokrane [7]	GFRP	Tensile	Concrete & saline solution	≤365	23, 40, 50, 70
Davalos et al. [16]	GFRP	Tensile	Concrete	≤270	20, 40, 50, 60
Robert et al. [6]	GFRP	Tensile	Concrete & tap water	≤240	23, 40, 50
Chen et al. [13]	C, & GFRP	Tensile, bond & horizontal shear	Tap water, alkaline sol. & simulated seawater	≤120	40, 60
Chen et al. [14]	GFRP	Tensile	Alkaline solution	≤240	20, 40, 60
Micelli and Nanni [11]	C, & GFRP	Tensile & horizontal shear	Alkaline sol., freeze-thaw & environmental expo.	≤42	−18, 4, 16, 27, 38, 49, 60
Benmokrane et al. [12]	GFRP	Tensile	Alkaline solution & concrete	≤90	23, 60
Dejke and Tepfers [4]	GFRP	Tensile	Alkaline solution, concrete & tap water	≤365	23, 40, 60

[a]GFRP (Glass FRP), BFRP (Basalt FRP), and CFRP (Carbon FRP).

strength. It was an experimental study and no service life predictions were conducted.

The exposure solutions, as well as the exposure durations and temperatures, vary significantly. Most of the studies exposed FRP rebars for less than one year, at an accelerating temperature ranging mainly between 23 °C and 60 °C. Submersion in alkaline solutions or embedment in different types of concrete were the predominant exposure conditions, followed by aging in simulated seawater. Some of the studies found in the literature combined the durability of GFRP rebars with other types of FRP rebar types, such as BFRP (basalt FRP), or CFRP (carbon FRP), also used as non-corrosive internal reinforcement in RC structures. The outcomes of these studies are used to compare or validate the findings of this research.

2. Problem statement and research significance

Many researchers have attempted to evaluate the durability of GFRP rebars by subjecting them to accelerated conditioning protocols (ACP), in which the rebars are exposed to different solutions (high pH, tap water, acid, etc.) at different temperatures, for different time periods, as summarized in Table 1. As coastal structures are one of the main targets for GFRP rebar applications [21], experiments and studies are needed that test and simulate the degradation, for example, on heavily cracked coastal structures, such that the durability of this rebar alternative can be more precisely description and quantified. This appears eminent because DOT agencies (e.g.; Florida DOT), did not allow the use of GFRP rebars in submerged conditions until this knowledge gap was filled through this research project.

To extend the durability knowledge and to deeper study degradation processes in GFRP rebars, additional mechanical properties, other than tensile strength, should be evaluated. In this study, tensile properties (maximum strength and elastic modulus) were evaluated since they are the main values used in design of FRP reinforced concrete structures. Moreover, the retention of horizontal and shear strength after exposure was also assessed, which can provide information about the durability of the fiber and resin, respectively. To visually analyze the potential degradation of the rebars after exposure with the goal of determining the degradation mechanism, the microscopic integrity of the rebar was evaluated via scanning electron microscopy (SEM). Finally, the interface between the rebar and concrete was appraised to assess the bond-to-concrete behavior over time; critical to ensure a proper composite action between the reinforcement and the concrete in RC structures.

Table 2
Characteristics of the evaluated GFRP rebar types.

ID	Cross section	Surface enhancement	Material	
			Resin	Fiber
Type-A	Round and Solid	Helical wraps + Sand-coating	Vinyl-ester	E-CR Glass
Type-B	Round and Solid	Helically grooved	Vinyl-ester	E-CR Glass
Type-C	Oval and Solid	Lugs	Vinyl-ester	E Glass
Type-D	Round and Solid	Helical mesh + Sand-coating	Vinyl-ester	E-CR Glass
Type-E	Round and Solid	Helically grooved	Epoxy	E-CR Glass
Type-F	Round and Solid	Helical wraps + Sand-coating	Vinyl-ester	E-CR Glass

Therefore, the novelty of this research project was three-fold: (i) the aging solution used for the accelerated aging was actual seawater taken directly from the ocean, providing more realistic conditions, (ii) multiple physio-mechanical properties were simultaneously evaluated, including tensile strength, modulus of elasticity, horizontal and transverse shear strength, and micro-structural composition, and (iii) the durability of the bond-to-concrete strength of six GFRP rebars with significant surface characteristics was evaluated.

3. Methodology

This research project was conducted to target an extensive evaluation of virgin and aged material properties of GFRP rebar products. Accordingly, products from six major GFRP rebar manufacturers were selected (Type-A through Type-F) to evaluate six of the most established GFRP rebar products worldwide. These manufacturers represent six of the most established GFRP rebar products worldwide, enabling a broader and more realistic analysis of the global GFRP industry. Table 2 summarizes the cross-sectional shape, surface enhancement and type of raw materials used for each of the rebar types. Most of the tested products were made from vinyl-ester and E-CR glass (which is an upgraded corrosion resistant version of traditional E-glass) except Type-C, which was made with E-glass, and Type-E, which was manufactured from epoxy resin. All the rebars were round and solid, with the exception of Type-C with an oval cross section. However, the surface enhancement varied significantly: three rebar types were sand coated (Type-A, Type-D, and Type-F), two featured helical grooves (Type-B and Type-E) and one had surface lugs (made from resin) similar to traditional black steel rebars (Type-C). Among the sand coated rebars, Type-A and Type-F rebars also featured helical wraps to bundle the fibers together and provide additional surface interlocking, while this effect was achieved through a double-helical mesh for Type-D rebars. Fig. 1 provides an

Fig. 1. GFRP rebars within the scope of the project. Type A through F (from left to right).

Table 3
Conducted test methods to evaluate virgin material properties of GFRP rebars.

Rebar Id.	Type of property	Characteristic	Test method
A, B, C, D, E, F	Physical	Cross-sectional area	ASTM D 798
		Fiber content by weight	ASTM D 2584
		Moisture absorption	ASTM D 570
		Microstructure observation[a]	SEM[a]
	Mechanical	Tensile strength	ASTM D 7205
		Modulus of elasticity	ASTM D 7205
		Transverse shear properties	ASTM D 7617
		Horizontal shear properties	ASTM D 4475
		Bond to concrete strength	ASTM D 7913

[a]Only rebar types A, B and C were tested.

overview of the geometrical features and surface enhancements for the six rebar types that were tested for this project. For each rebar test sample, four physical properties (fiber content by weight, cross-sectional dimensions, moisture absorption and micro-structural observation through Scanning Electron Microscopy or SEM) and five strength characteristics were measured, as noted in Table 3. For all the measured virgin characteristics, a minimum of five specimens per test group were tested.

3.1. Accelerated aging protocols

To assess the durability of GFRP rebars in seawater environments, additional virgin material samples were submerged in seawater at different temperatures and exposure times. In total, five mechanical properties (tensile strength, E-Modulus, transverse shear strength, horizontal shear strength, and bond strength) were evaluated for the aged samples to characterize the relative performance in reference to the (virgin) benchmark values. In addition, the micro-structure of the exposed rebars was also checked via SEM.

All samples were submerged in seawater tanks located at the marine laboratory of the Rosential School of Marine and Atmospheric Science (RSMAS) at University of Miami (Miami, Florida). This facility is located directly on the coast, allowing a direct supply of seawater from the bay. The tanks included an open circuit with a constant seawater stream to ensure the real-life conditions to which coastal structures are exposed. This was one of the main novelties of this study compared to others that exposed samples to simulated seawater by ASTM D1141 [22] instead of natural seawater [5,7,8,13,17,18,20]. As seen by other researchers, the effect of simulated solutions, such as simulated concrete pore solution, can efficiently be used to predict real-life environments, even though they are proven to be not 100% representative [4,12].

Table 4
Seawater chemical composition.

Ions	Concentration (ppm)
Na^{+}	10,735.7
K^{+}	380.0
Ca^{+2}	424.0
Mg^{+2}	1416.0
Cl^{-}	19,920.0
SO_4^{-2}	2697.0

Table 5
Test matrix for the accelerated aging protocol.

Phase	Rebar type	Accelerated conditioning protocol	
		Temp. °C	Time Days
I	A, B, C	23, 40, 60	60, 120, 210, 365
II	D, E, F	23, 60	

To avoid this issue and have a more realistic durability evaluation, natural seawater was used as exposure solution in this study. The chemical composition of the used seawater was obtained via inductively coupled plasma atomic emission spectroscopy (ICP-AES) and is presented in Table 4. An average pH value of 7.98 was recorded. More details of the composition are presented on parallel studies that also used seawater from Key Biscayne, Florida [15,23].

The water was heated using conventional 4 kW submergible heaters, and the temperature was constantly monitored using temperature data loggers. The seawater was heated to different temperatures to accelerate the potential degradation process and to evaluate the impact of different temperature intensities. Aging was achieved through two phases (Phase-I and Phase-II), as seen in Table 5. In total, the Accelerated Conditioning Protocol (ACP) included three temperatures (23 °C, 40 °C, and 60 °C and four different time periods (60 d, 120 d, 210 d, and 360 d). These temperatures were chosen because: (i) 23 °C resembles laboratory conditions, (ii) 60 °C is the most commonly used temperature for accelerated conditioning of FRP rebars [10,13] and because it has been proposed by ASTM D 7705 [24] for aging of GFRP rebars in alkaline water, and (iii) 40 °C provides reference values for cases in which extreme differences are observed between 23 °C and 60 °C. As defined in Table 5, Phase I samples were exposed to three temperature levels, while Phase II samples were aged at 23 °C and 60 °C because Phase I results reveled that the difference between the degradation in 23 °C and 40 °C was not significant, and therefore, the 40 °C condition was removed from the scope for economic and work-load reasons. The conditioning of test samples is illustrated in Fig. 2 and it can be seen that the samples were stored in different water baths to expose individual specimen groups to different conditions.

3.2. Specimen preparation and testing procedure

The specimen preparation and testing for each type of test was done according to the corresponding ASTM standards, listed in Table 3. The specimens used to determine the benchmark properties of the GFRP rebars within this project, were cut, prepared, conditioned and tested in laboratory conditions, while the test samples used to assess the durability were first exposed to seawater though the accelerated aging protocol. For the exposure, the 1.5 m long rebar sticks received directly from the manufacturer, were first sealed with epoxy at both ends (to avoid moisture diffusion from the cut ends), and were then submerged in seawater, 'naked', as seen in Fig. 2. Once they reached the aging period, they were removed from the tanks and cut to length to test the different mechanical properties after being aged. The only samples

(a) Storage tanks filled with specimens — overview

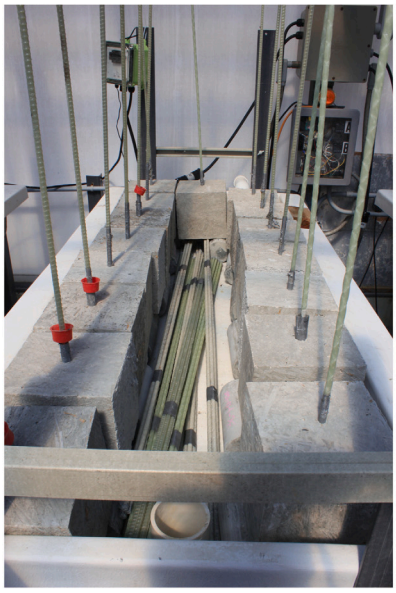

(b) Before exposure to temperature controlled seawater

(c) During exposure to temperature controlled seawater

Fig. 2. Specimen conditioning according to accelerated conditioning protocol.

that were prepared prior to being exposed to seawater were the bond samples, which were first cast according to ASTM D7913. The concrete used for the preparation of the bond specimens was the standard FDOT 'Type II 4500 Bridge Deck', with a 28-day compressive strength of 37.20 MPa (Standard deviation of 0.67 MPa and coefficient of variation of 1.8%).

4. Results

The six different rebar type samples were tested in a virgin state and after exposure to seawater at different temperature levels to quantify and evaluate the durability under different conditions. The results obtained from virgin state testing provided benchmark values (100%) such that property retention could be characterized throughout the durability evaluation.

4.1. Benchmark values

The results obtained from testing pristine rebars (benchmark values) are summarized in Tables 6 and 7. It was seen that the cross-sectional dimensions and fiber content were very comparable for the different rebars, while the long-term moisture absorption varied significantly: rebar Type-A absorbed about five times more moisture relative to the initial weight of the specimen than rebar types B, C, E and F, which had a similar behavior. Type-D rebars, however, measured values between

Table 6
GFRP rebar materials — Physical characteristics.

Rebar type	Cross-sectional area		Fiber content by weight		Moisture absorption	
	Avg mm^2	CoV %	Avg %	CoV %	Avg %	CoV %
A	81.0	2.6	76.3	0.5	1.16	4.2
B	86.1	1.4	84.1	0.1	0.19	3.7
C	80.0	3.9	76.1	0.1	0.22	3.5
D	89.9	1.0	70.1	0.4	0.76	3.1
E	91.1	6.1	81.6	0.4	0.25	2.1
F	83.0	1.0	70.9	0.8	0.20	2.7

Type-A and the remaining rebars, with a relative moisture uptake of approximately three times more than rebar types B, C, E and F. Overall, all the physical properties were within the accepted ranges as per the current standard specification for GFRP rebars, ASTM D7957 [25], except the moisture absorption for Type-A rebar, which exceeded the 1% saturation limit.

Table 7 summarizes the numerical findings for the evaluated mechanical characteristics that were considered within the scope of this research.

It can be seen that the properties of the different rebar types vary significantly. However, all of them reached the minimum strength values defined by ASTM D7957 [25]. Compared to the results for

Table 7
GFRP rebar materials — Mechanical characteristics.

Rebar type	Tensile strength		E-modulus		Transverse shear strength		Horizontal shear strength		Bond strength	
	Avg MPa	CoV %	Avg GPa	CoV %	Avg MPa	CoV %	Avg MPa	CoV %	Avg MPa	CoV %
A	953.8	5.5	51.6	5.1	212.4	4.8	42.9	7.7	18.4	11.9
B	830.1	6.6	61.2	3.2	157.0	6.5	43.7	5.9	18.8	10.1
C	982.5	4.3	54.6	6.0	211.2	2.6	50.3	5.6	22.3	12.0
D	1306.3	4.9	63.4	2.8	288.6	5.2	51.3	5.8	16.1	13.5
E	1058.0	2.5	56.9	3.3	248.6	3.8	41.6	2.6	14.5	14.3
F	1017.1	1.8	55.4	3.6	239.2	1.3	37.0	7.8	20.0	15.0

the physical properties, the variability, in this study evaluated by the coefficient of variance (CoV), is higher. This is attributed to the generally higher complexity of the specimen preparation and testing protocols for the evaluation of the mechanical properties. The bond strength was, among all, the most variable property; the fact that for the bond strength test an additional variable is added, the concrete, is believed to be the reason behind this higher variability.

From the results obtained by testing the rebars as received from the manufacturer, it was inferred that out of the six different rebar types evaluated within the scope of this research, all of them exceeded the minimum requirements set by the acceptance criteria except Type-A, which had a higher moisture absorption than the threshold set by ASTM D7957 [25]. Therefore, Type-A was considered a substandard rebar according to ASTM D7957. However, to assess the effect of excessive moisture uptake in the durability of GFRP rebars, Type-A was still included in the durability evaluation.

4.2. Durability evaluation

GFRP rebar specimens were exposed to saltwater solutions at three different temperatures (23 °C, 40 °C and 60 °C) for a duration of up to one year, in which specimens were removed and tested after four different time periods (60 d, 120 d, 210 d and 365 d). Accordingly, the graph presented in Fig. 3 plots the exposure duration on x-axis and the retention of the individual property (in %) along the y-axis, for the different rebar types and mechanical properties. The values indicated by each marker were calculated by averaging the ultimate capacity of at least three individually tested specimens. The standard deviation is not represented because it is an insignificant measure for three data points.

As expected, the higher temperature environment of 60 °C led to significantly more strength reduction than the two lower conditioning temperature levels (23 °C and 40 °C). It was seen that the durability of the different rebars varied significantly; overall Type-A rebars (substandard rebars according to ASTM D7957) suffered the most degradation, followed by Type-D rebars and then Type-B, Type-C, Type-E and Type-F rebars which showed comparable performance, and suffered lower deterioration. In general, the tensile strength was the mechanical property that measured the most significant degradation with a reduction of tensile capacity of up to approximately 45%, followed by the transverse shear and bond strength (20%), horizontal shear strength (10%) and E-modulus, for which the reduction was negligible. Excluding rebar Type-A, however, the tensile strength deterioration decreased to a maximum of 37.5% and 25% on average. The COV values summarized in Table 7 may indicate that what is considered degradation in Fig. 3 could be partially related to the scatter inherent to the variability of the test. Compared to studies that assessed the durability of the GFRP rebars by aging them under similar conditions [6,7,9,15,17,26], the retention values in this research appear comparable for rebars Type-B, Type-C, Type-E and Type-F, but Type-A and Type-D generally measured higher degradation.

It can be inferred that the degradation of the modulus was insignificant compared to the reduction of the maximum tensile capacity, even though both properties are related to the tensile behavior and are determined using the same test method (ASTM D7205). This has been reported by others before [6,7,17]. Even if the test method to assess both mechanical properties is the same, the tensile strength is related to the maximum tensile capacity at a critical strain prior to failure (at a strain of about 1.25% depending on the rebar type), while the E-Modulus is computed at the lower range of the stress–strain curve (between 0.1% and 0.3%). Currently, it is assumed that a degradation of the fiber and resin interface takes place, which affects the stress transfer between fibers. This reduction is more noticeable at critical strains (related to the maximum tensile strength) where the decrease in the stress transfer capacity may lead to the inability to activate all the fibers of the cross section of the rebar which results in higher strains in the critically engaged fibers. This will then cause failure of individual fibers at an earlier stage, leading to a premature failure of the rebar and reducing the ultimate tensile strength. However, since the elastic modulus is not related to individual or incremental fiber failures at a critical strain but rather to the sum of the elastic strain all along the coupon or rebar gage length (since it is computed at low strain), is not that significantly affected.

In addition, it is widely recognized [6,7,16,17] that the moisture uptake of GFRP rebars affects their durability. Comparing the tensile strength retention values to the moisture absorption results Summarized in Table 6, a correlation between both properties can be inferred. Among the six tested GFRP rebars, Type-A had the highest moisture absorption with around 1.5%, followed by Type-D (0.75%) and far above 0.2% for Type B, C, E and F. This same trend can be seen for the retention of tensile strength properties, which based on the outcomes of this research, leads to the conclusion that the higher the moisture absorption of a GFRP rebar, the lower the tensile strength retention after being exposed to seawater. No other significant correlation between the degradation and the rest of the physical properties presented in Table 6 was detected.

Finally, the degradation at the micro-structural level was assessed. Rebars Type A, B and C were tested using SEM image technology. Fig. 4 shows the SEM images for each of the three rebar types after exposure to seawater for 365 days at 23 °C, 40 °C, and 60 °C. The SEM pictures were taken from the different locations of the cross-section with a magnification of x50, with the objective to analyze the voids system and micro-structural density. In total, over 30 SEM pictures were taken per rebar type and size. It was seen that the void concentration was higher at the outer area of the cross-section than in the inner core, which was attributed to the production process, named pultrusion. This was also seen by Khatib et al. [15]. The ingress of moisture or other potential degrading agents comes from outside towards the center, being the outside pores more critical since they are the first ones to get filled. Therefore, the outer part of the rebar section was evaluated more in depth because it was assumed that the degradation initiates from the outside toward the rebar core, as the exposure solution penetrates the rebar.

Representative SEM images of the outer part of rebar types A, B and C after being aged in seawater for one year are shown in Fig. 4.

Among the three evaluated rebar types, Type-A was clearly the most porous rebar. These findings coincide with the moisture absorption values summarized in Table 6, being Type-A also the rebar with the highest moisture absorption. The magnification of the SEM

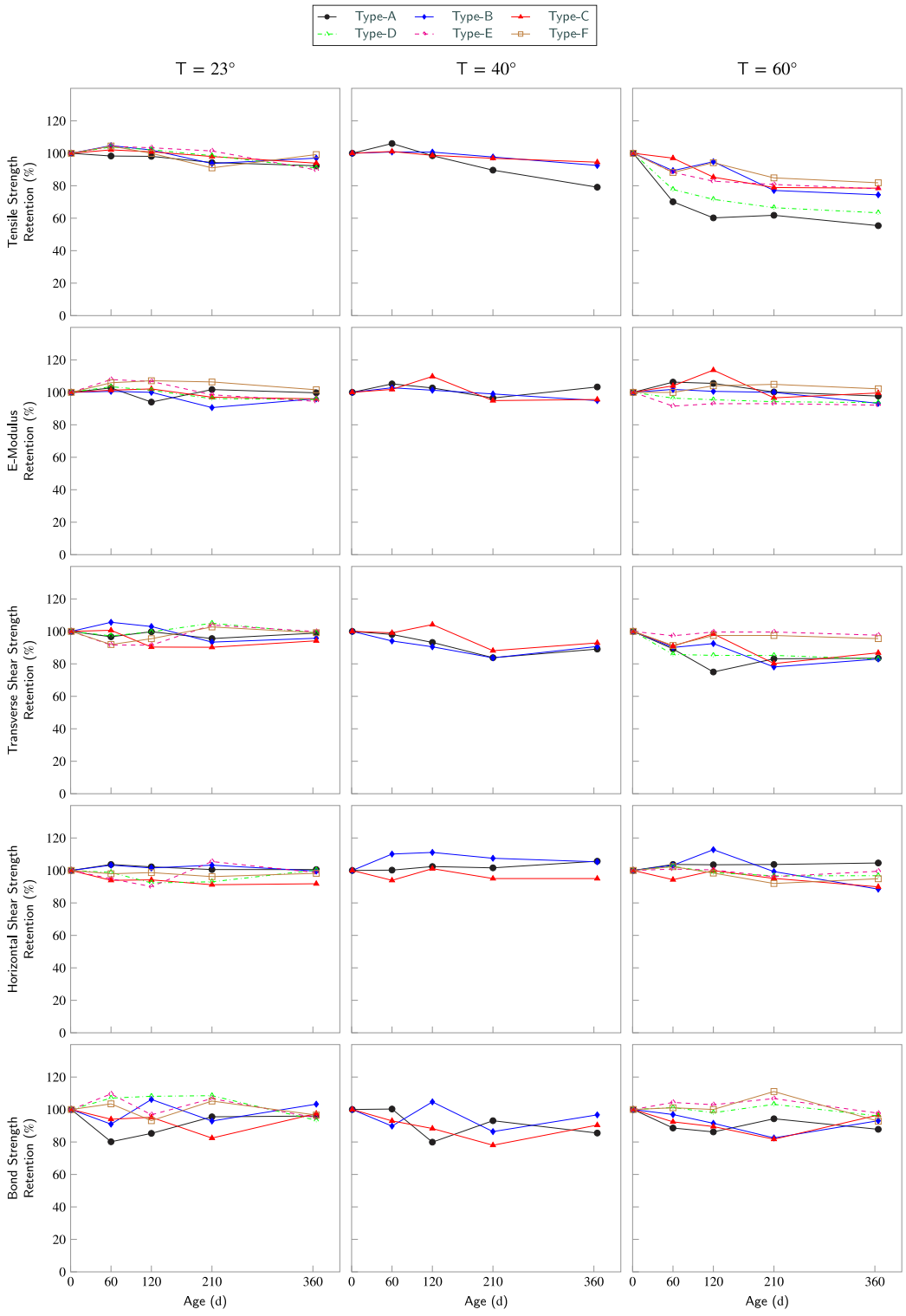

Fig. 3. Retention of the different mechanical properties over time while being exposed to seawater at 23 °C, 40 °C, and 60 °C.

images, however, was not high enough to determine the degradation mechanism from a micro-structural perspective.

Through strength retention analysis and failure mode observations for the different mechanical properties within the scope of this study, the deterioration of the fiber–resin interface was proposed as the principal mode of degradation, as discussed above. Other authors have also spoken to potential material lose (resin hydrolysis/fiber dissolution) in addition to the fiber–resin interface deterioration, as the reason for the decay of strength [15,16,27], but no material lose could be backed up with the SEM magnification used in this study.

5. Arrhenius model

The Arrhenius equation is a model proposed by Svante Arrhenius in 1889, developed to model the temperature dependent reaction rates of chemical processes. This equation supports the historically proven

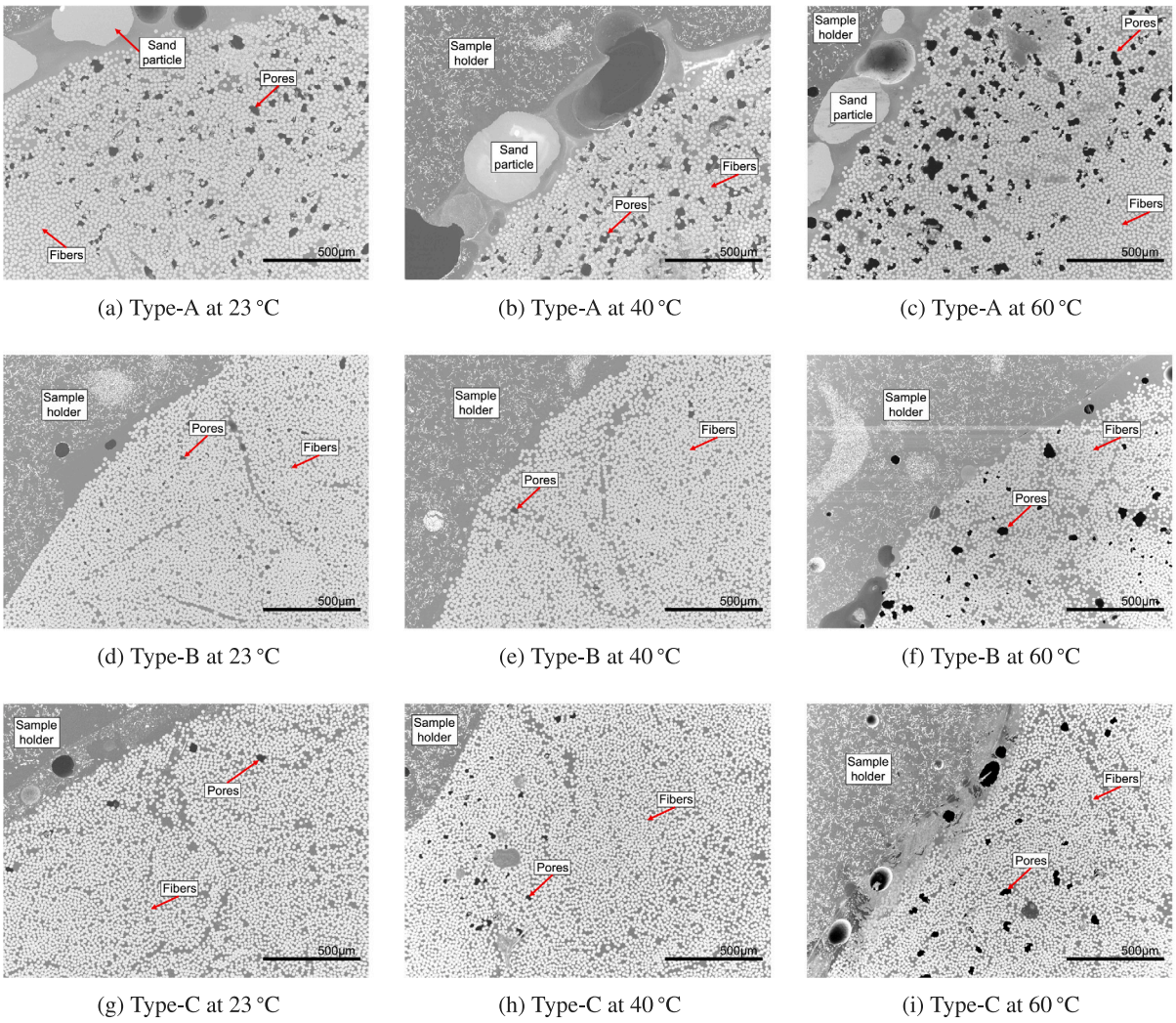

(a) Type-A at 23 °C (b) Type-A at 40 °C (c) Type-A at 60 °C

(d) Type-B at 23 °C (e) Type-B at 40 °C (f) Type-B at 60 °C

(g) Type-C at 23 °C (h) Type-C at 40 °C (i) Type-C at 60 °C

Fig. 4. SEM images for rebars Type A, B, and C (from top bottom) after being exposed to seawater for 365 days at 23 °C, 40 °C, and 60 °C (from left to right). Magnification: x50.

generalization that the rate of reaction at room temperature doubles every 10 °C for many chemical reactions [28]. The general Arrhenius relationship is expressed in Eq. (1),

$$k = A_0 e^{\frac{-E_a}{RT}} \tag{1}$$

where: k is the rate coefficient ($\mathrm{mol\,L^{-1}}^{\frac{1-n}{s}}$), T the absolute temperature, (K), A_0 is the pre-exponential or Arrhenius factor (constant for every chemical reaction) ($\frac{\mathrm{L}}{\mathrm{mol}\ s}$), R the universal gas constant ($\frac{\mathrm{J}}{\mathrm{mol\ K}}$), and E_a is the activation energy for the reaction to happen ($\mathrm{J\,mol^{-1}}$).

By applying natural logarithms to both sides of the equation, the general Arrhenius equation can be transformed into the following linear expressions (see Eq. (2)), which clarifies the relationship for improved interpretation. When this expression is plotted, the Arrhenius Plot is obtained.

$$\ln\left(\frac{1}{k}\right) = \frac{E_a}{R}\frac{1}{T} - \ln A \tag{2}$$

It can be seen that the logarithm of the time needed for a material property to reach a certain value is a linear function of $\frac{1}{T}$ with the slope $\frac{E_a}{R}$. Hence, E_a/R and A can be calculated from the slope of the regression together with the point of intersection between the regression and the y-axis of the Arrhenius Plot.

The data obtained from accelerated aging protocols can be used for the Arrhenius model to calculate and predict the long-term behavior of FRP rebars. To evaluate the material deterioration via the Arrhenius model, a single predominant deterioration mechanism must be assumed, and should not change with time or temperature throughout exposure; the rate of degradation should only be accelerated through increased temperatures. In addition, no post curing or little effect of the post curing of the resin is assumed due to the temperature of the accelerated conditioning protocols. In this study, the degradation rate (needed for the Arrhenius model) was calculated by using four mathematical models commonly used in the literature to assess the degradation of GFRP rebars: (i) single logarithmic model, (ii) double logarithmic model, (iii) exponential model, and (iv) moisture diffusion model. Each of these models are described next for the data obtained throughout the experimental phase.

5.1. Single logarithmic model

The single logarithmic model was developed by Litherland et al. [29], who successfully predicted the degradation of glass fiber concrete (GFC). It was then first introduced in the world of composite rebars by Bank et al. [30]. This model adopts a linear relationship between the strength retention (Y) and the logarithm of the time (t), as shown in Eq. (3), being a and b regression constants.

$$Y = a \log t + b \tag{3}$$

Since it was first introduced by Bank et al. [30], this model has been widely used by other researchers [4–7]. However, some research studies found no parallelism between the degradation plots at different

temperatures, which is the indicative inherent to his model to prove that the degradation mechanism remains unaltered with the increase of the temperature (as assumed by the Arrhenius model) [31,32].

5.2. Double logarithmic model

The double logarithmic model is a modified version of the single logarithmic model. It was proposed by Dejke and Tepfers [4] and introduces a second logarithmic scale along the *y*-axis, in addition to the already proposed logarithmic x-scale, suggested by Litherland et al. [29] (see Eq. (4)).

$$\log Y = a \log t + b \tag{4}$$

Dejke and Tepfers [4] showed that the results were comparable, or slightly improved using a double logarithmic scale. Other researchers were also able to apply this technique successfully [33–35] for different FRP rebars and exposure conditions. This model was also used to determine the environmental strength reduction factor ($\eta_{env,t}$) used in Fib bulletin 40 [36], equivalent to the $1/C_E$ in the ACI 440.1R-15 [37,38].

5.3. Exponential model

This model was proposed for the first time by Phani and Bose [39] and Phani and Bose [40] to predict flexural strength retentions using acousto-ultrasonic techniques. It was then modified to predict the tensile strength retention of GFRP and BFRP rebars exposed to high alkalinity solutions (see Eq. (5)), where Y_∞ is the retention at time infinity, and τ is the exponential constant dependent on temperature [14,16,31].

$$Y = (100 - Y_\infty)\ exp(-t/\tau) + Y_\infty \tag{5}$$

While the two logarithmic models presented above are not associated to any specific degradation mechanism, the degradation mechanism for the exponential models is assumed to model debonding at the fiber/resin interface [8], which was the degradation mode defined for the rebars within the scope of this project based on the durability results and SEM images. Compared to the logarithmic models, no parallelism requirements exists in this model because the model consists of an exponential mathematical expression, so the appropriateness of this model was assessed uniquely by checking the coefficients of determination or R^2 values.

5.4. Moisture diffusion model

The moisture diffusion models have been used in different applications throughout the last decades [41]. These models are based on different diffusion laws, such as Fickian model, Two-stage model, Langmuir's model, etc., but the Fickian law is the most frequently used one [41]. It is applied to correlate the strength retention with the moisture absorption of FRP rebars and it was first proposed by Saadatmanesh and Tannous [42]. Among the four evaluated degradation models, this latter one is the least used for FRP rebars because it is considered too conservative: it implies that the moisture-affected area is completely degraded and thus cannot carry load, although it is more likely that it is affected but still provides residual strength capacity.

The most frequently used expression of the Fickian diffusion model is shown in Eq. (6), were r_0 is the initial radius of the rebar, t is time, D is the diffusion coefficient, and C is the concentration of the solution.

$$Y = 100\left(1 - \frac{\sqrt{2DCt}}{r_0}\right)^2 \tag{6}$$

One of the limitations of this expression is the quantification of the concentration value, C. This is not an issue if the aging solution is a simulated alkaline or saline environment because a determined amount of chemicals are used to target a specific concentration. For seawater exposure, however, many chemicals, bacteria, and other potential damaging agents exist, which complicate the determination of the concentration. This also applies to samples exposed to regular tap water, where no principal chemical exists. To overcome this limitation in this study, a modified version of the Fickian model, proposed by Davalos et al. [16], was used (Eq. (7)), which incorporates parameters (j and α) that account for temperature effects, solution concentration, and other experimental conditions; if $\alpha = -0.5$, Eq. (7) becomes equivalent to the general prediction model based on moisture absorption (Eq. (6)).

$$Y = 100\ \left(1 - jt^{\alpha+1}\right)^2 \tag{7}$$

6. Service life prediction

The goal of the durability model is to predict the long-term behavior of GFRP rebars to properly anticipate the service life of such rebars in saltwater environments. Accordingly, the four different degradation models to determine the degradation rate (presented above) were evaluated, and the Arrhenius equation was used to model the effect of the temperature. In total, five different physio-mechanical properties (tensile strength, elastic modulus, transverse and horizontal shear strength, and bond-to-concrete strength) were taken into account and addressed throughout the service life prediction.

6.1. Degradation rate

First, the four degradation models were fitted to the experimental data and the appropriateness of each of the models was assessed. By applying the single logarithmic model, it was seen that most of the trend lines for the different rebar types and mechanical properties were not parallel among themselves, which according to the model meant that the degradation rate changed with the temperature and, therefore, the use of the Arrhenius model was invalidated [31,32]. In addition, the R^2 values, which evaluate the fit of the degradation model to the experimental data, varied significantly but in general were very low (as low as 0.003) compared to those values found in the literature that successfully applied this model (all over 0.8) [4–7], which indicated a lack of correlation among the data points in each set when using this model. Only the tensile strength retention values showed acceptable R^2 values, since they were all recorded beyond 0.75, but the parallelism between the trend lines was not maintained.

When applying the double logarithmic model, no main difference was seen in the adequacy of the model fit compared to the results obtained with the single logarithmic model. In this case too, a general lack of parallelism within the different trend lines for each condition was observed and the R^2 values were relatively low. The tensile strength retention was the only "exception", similar to the results obtained with the single logarithmic model. Single and double logarithmic models appear to be the most popular models among researchers to model the degradation of FRP rebars for the various mechanical properties. However, some intrinsic limitations exist in these models as also pointed out by Davalos et al. [16] and Wang et al. [17]: the main issues are that (i) no degradation mechanism is attributed to these models [38] and (ii) that the residual strength approaches infinity at exposure time zero, which does not correlate with the real test data (as it should converge to 100% at time zero). Within the scope of this study, a modified variation of these two models was tested: an additional data point of 100% retention at time zero was added. This however, violated parallelism requirements between the plots because each data set was forced to pass through that same initial point. In addition, the R^2 values were reduced significantly (two to three times lower on average), resulting in an insignificant fit.

The third model that was checked was the exponential model. As reference, Fig. 5 shows how the experimental data for the tensile strength retention obtained throughout this research project was applied and fitted to the model, as a visual reference.

Each of the six graphs represent a particular rebar type. The tensile strength percentage retention is plotted along the *y*-axis, while

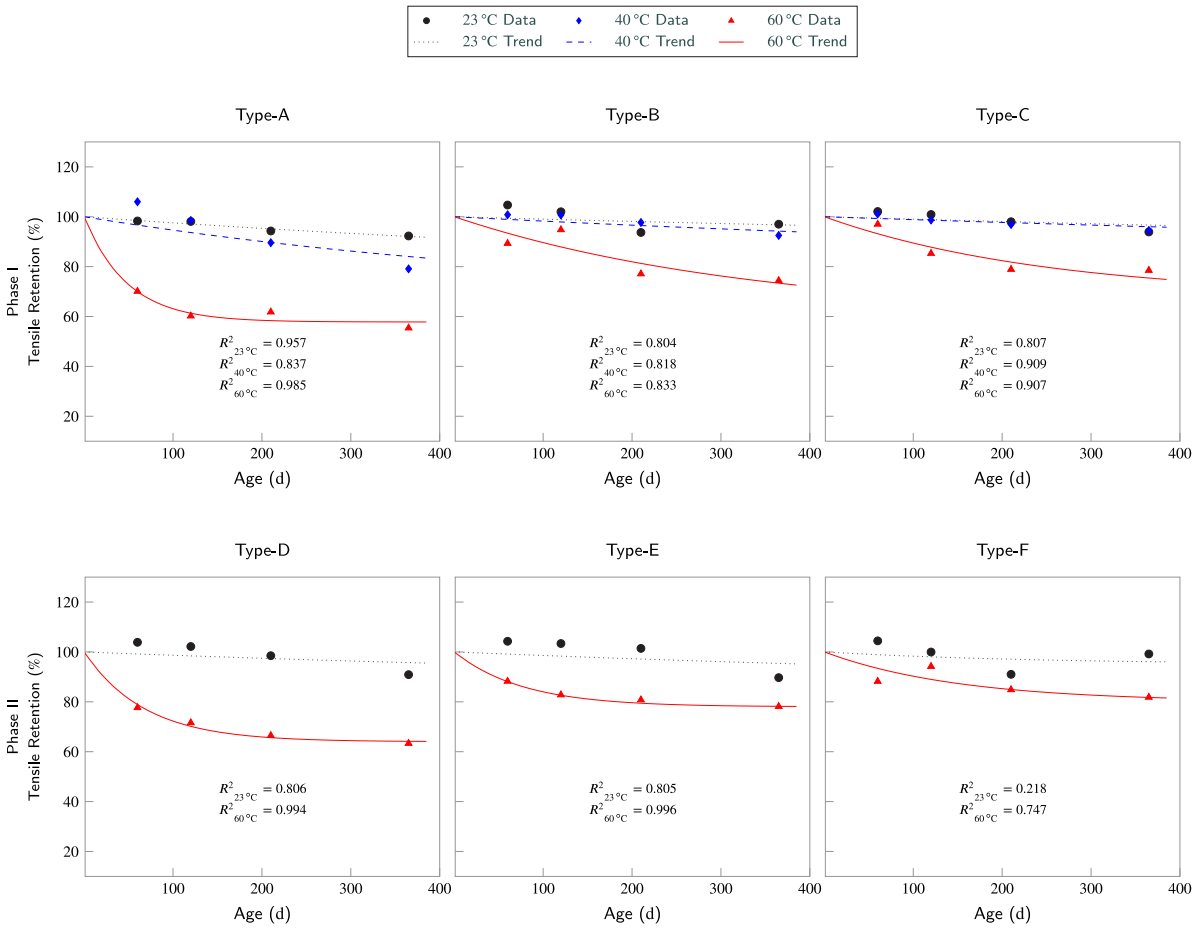

Fig. 5. Exponential degradation model fitted to the tensile strength retention values.

the exposure duration/age is represented on the x-axis in days. For reference, the R^2 values are listed with in each graph. Compared to the two logarithmic models, the R^2 values were slightly improved, and for all rebar types the tensile strength was the mechanical property that produced the best fit. However, to determine whether the temperature only increases the degradation rate without changing the degradation mechanisms, the Arrhenius plots, need to be evaluated.

The fourth and last model that was checked was the moisture diffusion model. Following the same trend as seen with the previous three models, the R^2 values varied significantly and were low in general, and for each and all rebar types, the tensile strength was the mechanical property that produced the best fit.

6.2. Arrhenius plot

After the degradation rates were modeled through the four different degradation models evaluated, as presented in the previous section, the Arrhenius model was applied. It was found that the tensile strength only showed an acceptable fit for the evaluated degradation models. Therefore, the other properties could not be considered for the application of the Arrhenius model and it was decided that only the retention of the tensile strength would be further considered.

From Eq. (2), it can be seen that the logarithm of the required time for a material property to reach a certain value is a linear function of $\frac{1}{T}$ with a slope of $\frac{E_a}{R}$. Hence, $\frac{E_a}{R}$ and A can be calculated from the slope of the regression and from the point of intersection between the regression and the y-axis, respectively. The activation energy (E_a) is a fundamental characteristic for every chemical reaction. It defines the minimum energy that is required for a chemical reaction to occur. If the chemical reaction does not change with the temperature (as assumed by this model) and the degradation rate is correctly modeled, then the energy needed to reach a certain degradation level should be the same for each of the different temperatures, but the time to reach that degradation will change (the pre-exponential or Arrhenius factor A will vary). This assumption is, therefore, proven by plotting the Arrhenius plots and checking the activation energy at each of the analyzed degradation levels. Following the modified Arrhenius expression (Eq. (2)), the activation energy can be calculated from the slope of the Arrhenius plot, because if the activation energy should remain constant, then the plots (related to different degradation levels) should show identical slopes, and therefore, must be parallel.

Three degradation levels were selected: 95 %, 90% and 85 %. For every rebar type (Type-A through F) the plots related to these three degradation levels for each of the four degradation laws (single logarithmic, double logarithmic, exponential and diffusion model) were analyzed. Though in the previous section it was seen that the requirements that validate the use of the single and double logarithmic models were not met (no parallelism was seen), these two models were still included in the evaluation of the Arrhenius model because it appears that the requirement for parallelism is too limiting for the degradation model, and that the effect of the temperature should actually be checked by evaluating the parallelism of the Arrhenius plots and not the parallelism of the degradation plots.

For the rebar types within the scope of Phase-I, three sets of data points were plotted (relative to the three exposure temperatures), while two data sets were plotted for the rebars of Phase-II (rebars exposed to two temperatures). Then, a linear trend line for each of the degradation levels was fitted through the data sets: for the Phase-I rebars the coefficient of determination (R^2) was checked to evaluate the fit of the trend line to the three points relative to the different temperatures,

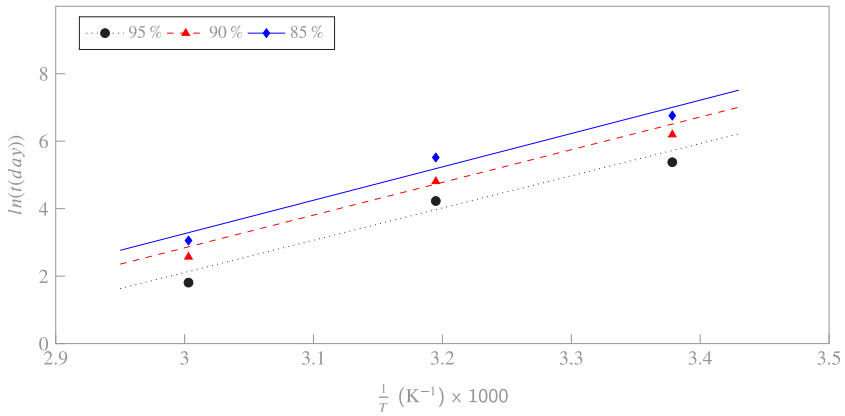

Fig. 6. Arrhenius plot for Type-A.

Table 8
Activation energy and R^2 values for tensile strength retention based on the exponential model.

Rebar type	Retention					
	95%		90%		85%	
	E_a K	R^2 –	E_a K	R^2 –	E_a K	R^2 –
Type-A	9545.4	0.91	9685.0	0.93	9891.9	0.95
Type-B	6484.0	0.90	6283.8	0.90	6053.7	0.91
Type-C	6183.5	0.78	5843.9	0.78	5704.1	0.78
Type-D	8684.4	1.00	8749.5	1.00	8437.5	1.00
Type-E	6883.8	1.00	7107.1	1.00	6913.1	1.00
Type-F[a]	4961.1	1.00	–	–	–	–

[a]The prediction for Type-F rebars at 23 °C yields to 92.1% of retention so no prediction for 90 or 85% could be done. Therefore,the following alternative retentions were evaluated: E_a/R (97.5%) = 5244.1 K, E_a/R (95.0%) = 4961.1 K, and E_a/R (92.5%) = 5044.3 K.

Table 9
Long-term retention values.

Rebar type	Temperatures					
	23 °C		40 °C		60 °C	
	Y_∞ (%)	t (years)	Y_∞ (%)	t (years)	Y_∞ (%)	t (years)
Type-A[a]	73.3	24.5	65.1	11.2	57.8	1.1
Type-B	84.7	26.2	78.3	16.4	70.1	3.4
Type-C	82.8	25.3	76.6	15.2	70.2	2.9
Type-D	81.1	27.3	–	–	63.1	1.4
Type-E	84.3	27.8	–	–	74.2	2.1
Type-F	92.1	23.2	–	–	78.3	2.3
Average[b]	85.9 ± 4.0	26.0 ± 1.8	77.5 ± 1.2	15.8 ± 0.8	71.0 ± 5.7	2.4 ± 0.8

[a]Substandard rebar type according to ASTM D7957 due to excessive moisture uptake.
[b]Average values of all rebar types except rebar Type-A.

while the R^2 values were equal to 1.0 for rebars of Phase-II as only two points were correlated. As visual example, Fig. 6 shows the Arrhenius plots for the tensile strength degradation of Type-A rebar based on the exponential degradation model. For each of the different rebar types and degradation models, the activation energies for all retention percentages (95 %, 90% and 85 %) were compared to evaluate the parallelism among the Arrhenius plots. The exponential degradation law appeared to be the model that showed the highest parallelism among the plots for each of the rebar type with $\frac{E_a}{R}$ values that had a maximum difference of 7% among themselves (see Table 8). This was followed by the single logarithmic model (about 30% max. difference) and the double logarithmic model (about 40% max. difference). The diffusion model had the least parallel plots per rebar type and degradation model, with $\frac{E_a}{R}$ values with a difference of up to six times among themselves, specially for rebars Type-F and Type-C. Therefore, this last approach was not consider appropriate to model the degradation of the rebars tested in this research project after being exposed to seawater at different temperatures.

Based on the results obtained from the model fitting, the single and double logarithmic models were also found not to be appropriate for the data obtained in this project due to the lack of parallelism in addition to the limiting factor that the predictions yield to infinity at time zero and that no degradation mechanism is attributed to the model. The exponential model, however, met the two criteria to be accepted: (i) it showed an appropriate fit (all the R^2 values were above 0.8 except for Type-F) to the experimental data when evaluating the degradation rate, and (ii) the Arrhenius plots computed for this model were parallel for the different retention levels. This, added to the fact that the exponential method is based on the resin/interface debonding degradation mode (same failure mode as predicted for the rebars within the scope of this research), made the exponential model be the most appropriate degradation model among the four evaluated models in this study. Therefore, the exponential model uniquely qualified to predict the service life of the different rebar types when exposed to seawater.

Among the five analyzed mechanical properties (tensile strength, E-Modulus, transverse shear, horizontal shear and bond strength), only the values for the tensile strength retention were successfully modeled. No clear degradation trend was detected for the other four mechanical properties, which lead to the conclusion that none of the presented approaches truly qualify to predict the service life of GFRP rebars for such mechanical properties when exposed to seawater.

6.3. Predictive model

The service life prediction for the six different rebar types that were considered for this project was completed based on the exponential degradation model. Fig. 7 shows the service life prediction for the six different rebars for each of the evaluated temperature. Only tensile strength retention values were used to predict the service life of GFRP rebars, due to the described limitations of the degradation models and the inconstancy for modeling the degradation rate of transverse/horizontal shear, E-Modulus and bond strength properties. According to this model, a rapid degradation exists at the beginning of the service life of the evaluated GFRP rebars, converging to a long-term retention value, Y_∞, as determined by Eq. (5). The long-term retention values and the time to reach that convergence for each of the rebar type and temperature are summarized in Table 9.

Fig. 7 substantiates the initial assumption that the retention of the tensile strength is reduced with increased temperatures. Based on this model, in seawater-submerged conditions at a temperature of 23 °C, most of the rebars would retain a tensile strength of 80% over the service life of the structure, except rebar Type-A, for which a retention of

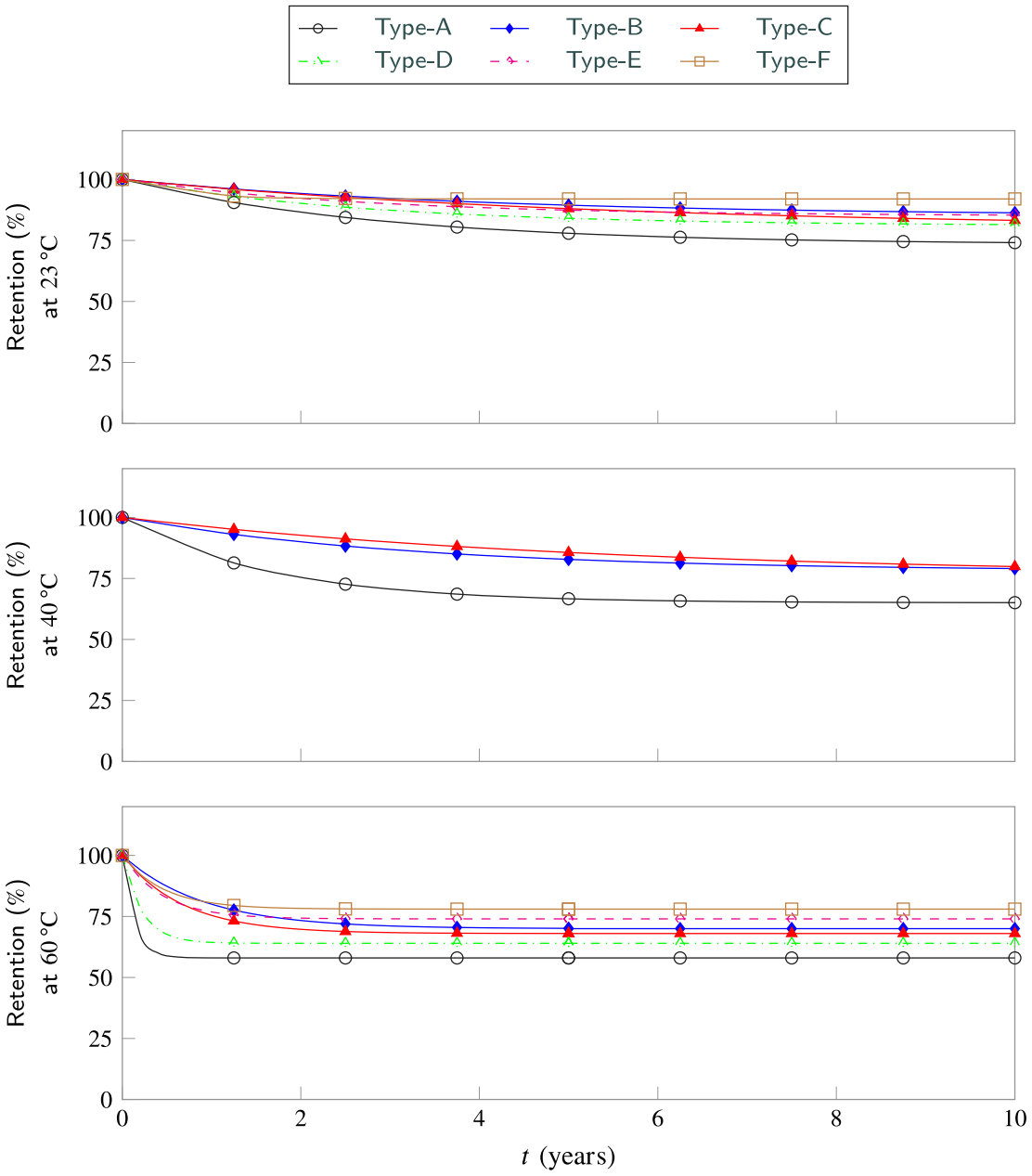

Fig. 7. Service life prediction (based on the exponential degradation model).

73.3% was predicted. However, it needs to be noted that Type-A rebar was defined as a substandard rebar according to ASTM D7957 due to excessive moisture uptake. If submerged in seawater at a temperature of 40 °C, for rebars Type-B and Type-C a retention more than 75% was predicted, while the retention for Type-A rebars would be 65.1% based on this model. Finally, at 60 °C, rebars Type-A and Type-B showed the lowest long-term predicted strength retention with 57.8% and 63.1%, respectively, while for the rest of the rebars a strength retention of 70% or above was predicted. The convergence times were comparable for all rebars within the same temperature level but were reduced as the aging temperature increased or the degradation rate was accelerated. At 23 °C the reduction of the tensile strength capacity was foreseen to occur within the first 23–28 years for all the rebars, at 40 °C within the first 11–15 years and at 60 °C within the first 1.1 to 3.4 years.

Finally, the average service life of GFRP rebars without considering rebar Type-A (substandard rebar according to ASTM D7957) was evaluated. At any of the exposure temperatures, a minimum retention of over 70% was predicted, being the average retention at 23 °C and 40 °C of 85.9% and 77.5%, respectively (see Table 9)

7. Implementation of research findings

To account for this reduction of capacity of GFRP rebars over time in the design of GFRP reinforced concrete structures, the American Concrete Institute incorporates an environmental reduction factor (C_E) in the 440.1R-15 specification, "Guide for the Design and Construction of Structural Concrete Reinforced with Fiber-Reinforced Polymer Bars" [37]. This factor is multiplied by the guaranteed tensile strength to obtain the design tensile strength that is meant to be used for all design equations. This factor was determined based on the consensus of the ACI 440 Committee and it takes a value of 0.7 (retention of 70%) or 1.0 (retention of 100%) for GFRP rebars, depending on the exposure conditions; 0.7 for concrete structures exposed to earth and water and 1.0 for no such exposure.

Based on the predictions of this study, the currently accepted C_E value of 0.7 for structures exposed to earth and water [37], appears to be too conservative. According to the NASA Earth Observations (NEO), the highest punctual sea surface temperature registered worldwide is about 35 °C, and the yearly average seawater temperature ranges between 20 °C and 27 °C in the Caribbean Sea, Mediterranean Sea or Persian Gulf (locations with considerable deployment of this technology). Therefore, the predictions at 60 °C are too extreme for coastal applications. Predictions at 23 °C could be considered the most adequate among the three temperatures evaluated in this study, being the predicted retentions at 40 °C also on the high end. At 23 °C, an average C_E value of 0.86 was obtained. This value is aligned with the results obtained by Benmokrane et al. [43], who re-evaluated the C_E value based on durability data from multiple projects found in the literature. However, to prove the validity of these outcomes and calibrate the model, these predictions should be compared to data obtained from existing structures that have been in service for an extended period.

8. Conclusions

In this study, the durability of six different rebar types was assessed based on the experimental data that was collected from mechanical testing of aged GFRP specimens. The rebars were exposed to natural seawater obtained directly from the bay at Key Biscayne, Florida. The durability was evaluated by testing rebars prior and after being exposed at various temperatures (23 °C, 40 °C and 60 °C) for different time periods (60, 120, 210 and 365 days). The durability of these GFRP rebars was assessed by evaluating changes in six different physio-mechanical properties, including: tensile strength, modulus of elasticity, transverse shear strength, horizontal shear strength, micro-structural composition and lastly, bond strength. In total, four different prediction models were evaluated to study the degradation rate of the GFRP rebars (single logarithmic, double logarithmic, exponential and diffusion model) and the Arrhenius equation was used to analyze the temperature effect and to predict the service life. Based on the analysis, results, and findings presented above, the following conclusions can be drawn:

- All rebar types exceeded the minimum requirements set by the acceptance criteria ASTM D7957 except Type-A which showed an excessive moisture absorption.
- The durability of different rebar types varies significantly. Particularly, in this study Type-A rebars were the most affected, followed by Type-D, whereas Type-B, Type-C, Type-E and Type-F showed comparable behavior with low deterioration.
- GFRP rebar durability appears to be proportional to the moisture absorption properties of the rebar: the higher the moisture uptake, the greater the degradation suffered. Moisture absorption measurements are indicative of long-term performance.
- Seawater exposure depredates GFRP rebars and leads to strength reduction. It appears that the tensile strength suffers most capacity reduction with up to 45%, followed by the transverse shear and bond strength (20%), whereas the horizontal shear strength (10%) and E-modulus do not suffer noticeable reduction. Excluding rebar Type-A (substandard rebar according to ASTM D7957 due to excessive moisture uptake), however, the tensile strength deterioration decreased to a maximum of 37.5% and 25% on average.
- Based on the strength retention values and failure modes, it was concluded that the fiber/resin interface is the main degradation mechanism.
- The service life prediction based on the Arrhenius model was only successfully applied for tensile strength retention values.
- The exponential degradation model had the best fit to the data, and the Arrhenius plots based on this model showed a considerable parallelism; this meant that the degradation mechanism was unaltered with the temperature, and was only accelerated. Therefore it was the chosen model to predict the service life of GFRP rebars.
- At 23 °C, all the rebars that met the acceptance criteria by ASTM D7957 are expected to retain 85% of the tensile strength capacity. Under more critical conditions (40 °C and 60 °C), a retention of 77.5% and 71% was predicted on average, respectively.
- Based on the predictions of this study, the currently accepted C_E value of 0.7 for structures exposed to earth and water, appears to be too conservative.

CRediT authorship contribution statement

Alvaro Ruiz Emparanza: Conceptualization, Methodology, Formal analysis, Writing – original draft. **Raphael Kampmann:** Software, Data curation, Visualization, Writing – review & editing. **Francisco De Caso:** Investigation, Resources, Writing – review & editing. **Carlos Morales:** Investigation, Writing – review & editing. **Antonio Nanni:** Supervision, Investigation, Writing – review & editing.

Declaration of competing interest

The authors declare that they have no known competing financial interests or personal relationships that could have appeared to influence the work reported in this paper.

Data availability statement

Some or all data, models, or codes that support the findings of this study are available from the corresponding author upon reasonable request.

Acknowledgments

The Authors would like to acknowledge the Florida Department of Transportation (FDOT) for funding under Project No. BDV30 TWO 977-18, in particular Chase C. Knight, Ph.D. and Steven Nolan, P.E. The statements made herein are solely the responsibility of the authors.

Appendix A. Supplementary data

Supplementary material related to this article can be found online at https://doi.org/10.1016/j.conbuildmat.2022.127028.

References

[1] A. Ruiz Emparanza, R. Kampmann, F. De Caso y Basalo, State-of-the-practice of FRP rebar global manufacturing, in: CAMX: The Composite and Advanced Materials Expo, Orlando, Florida, 2017.
[2] A. Nanni, A.D. Luca, H.J. Zadeh, Reinforced Concrete with FRP Bars: Mechanics and Design 978-0-415-77882-4, CRC Press, 2014, pp. 23–33, URL: http://www.crcnetbase.com.proxy.lib.fsu.edu/doi/pdfplus/10.1201/b16669-4.
[3] L.A. Escobar, W.Q. Meeker, A review of accelerated test models, Statist. Sci. 21 (4) (2006) 552–577.
[4] V. Dejke, R. Tepfers, Durability and service life prediction of GFRP for concrete reinforcement, in: Proc., 5th Int. Conf. on Fiber-Reinforced Plastics for Reinforced Concrete Structures (FRPRCS-5), Vol. 1, Thomas Telford London, 2001, pp. 505–516.
[5] Z. Dong, G. Wu, B. Xu, X. Wang, L. Taerwe, Bond durability of BFRP bars embedded in concrete under seawater conditions and the long-term bond strength prediction, Mater. Des. 92 (2016) 552–562, http://dx.doi.org/10.1016/j.matdes.2015.12.066.
[6] M. Robert, P. Cousin, B. Benmokrane, Durability of GFRP reinforcing bars embedded in moist concrete, J. Compos. Constr. 13 (2) (2009) 66–73.
[7] M. Robert, B. Benmokrane, Combined effects of saline solution and moist concrete on long-term durability of GFRP reinforcing bars, Constr. Build. Mater. 38 (2013) 274–284, http://dx.doi.org/10.1016/j.conbuildmat.2012.08.021, URL: http://ac.els-cdn.com/S0950061812006046/1-s2.0-S0950061812006046-main.pdf?{_}tid=e1e48d6e-4ad7-11e7-855e-00000aacb35d{&}acdnat=1496767852{_}577eeb81cc9b5b9432871c3752ae5b5b.
[8] Z. Wang, X.L. Zhao, G. Xian, G. Wu, R.K. Singh Raman, S. Al-Saadi, Durability study on interlaminar shear behaviour of basalt-, glass- and carbon-fibre reinforced polymer (B/G/CFRP) bars in seawater sea sand concrete environment, Constr. Build. Mater. 156 (2017) 985–1004, http://dx.doi.org/10.1016/j.conbuildmat.2017.09.045.

[9] B. Benmokrane, F. Elgabbas, E.A. Ahmed, P. Cousin, Characterization and comparative durability study of glass/vinylester, basalt/vinylester, and basalt/epoxy frp bars, J. Compos. Constr. 19 (6) (2015) 4015008.

[10] B. Benmokrane, A.H. Ali, H.M. Mohamed, A. ElSafty, A. Manalo, Laboratory assessment and durability performance of vinyl-ester, polyester, and epoxy glass-FRP bars for concrete structures, Compos. B 114 (2017) 163–174, http://dx.doi.org/10.1016/j.compositesb.2017.02.002.

[11] F. Micelli, A. Nanni, Durability of FRP rods for concrete structures, Constr. Build. Mater. 18 (7) (2004) 491–503, http://dx.doi.org/10.1016/j.conbuildmat.2004.04.012, URL: http://ac.els-cdn.com/S0950061804000601/1-s2.0-S0950061804000601-main.pdf?{_}tid=d12a6612-4cc9-11e7-b2d4-00000aab0f6b{&}acdnat=1496981714{_}d932be22882e5cd85da3095714e046d2http://go.galegroup.com.proxy.lib.fsu.edu/ps/i.do?p=GRGM{&}u=tall85761{&}id=GALE{%}7CA12232644.

[12] B. Benmokrane, P. Wang, T.M. Ton-That, H. Rahman, J.-F. Robert, Durability of glass fiber-reinforced polymer reinforcing bars in concrete environment, J. Compos. Constr. 6 (3) (2002) 143–153, http://dx.doi.org/10.1061/(ASCE)1090-0268(2002)6:3(143), URL: http://ascelibrary.org.proxy.lib.fsu.edu/doi/pdf/10.1061/{%}28ASCE{%}291090-0268{%}282002{%}296{%}3A3{%}28143{%}29.

[13] Y. Chen, J.F. Davalos, I. Ray, H.Y. Kim, Accelerated aging tests for evaluations of durability performance of FRP reinforcing bars for concrete structures, Compos. Struct. 78 (1) (2007) 101–111, http://dx.doi.org/10.1016/j.compstruct.2005.08.015, URL: http://ac.els-cdn.com/S0263822305002254/1-s2.0-S0263822305002254-main.pdf?{_}tid=75e863b2-4cc9-11e7-96b1-00000aab0f6c{&}acdnat=1496981560{_}f6fbf30ff996e1d5269980f9aac4fd4d.

[14] Y. Chen, J.F. Davalos, I. Ray, Durability prediction for GFRP reinforcing bars using short-term data of accelerated aging tests, J. Compos. Constr. 10 (4) (2006) 279–286.

[15] M. Khatib, S. Ramanathan, P. Suraneni, A. Nanni, Durability of commercially available GFRP reinforcement in seawater-mixed concrete under accelerated aging conditions, J. Compos. Constr. 24 (2020) http://dx.doi.org/10.1061/(ASCE)CC.1943-5614.0001035.

[16] J.F. Davalos, Y. Chen, I. Ray, Long-term durability prediction models for GFRP bars in concrete environment, J. Compos. Mater. 46 (16) (2012) 1899–1914.

[17] Z. Wang, X.-L. Zhao, G. Xian, G. Wu, R.K.S. Raman, S. Al-Saadi, A. Haque, Long-term durability of basalt-and glass-fibre reinforced polymer (BFRP/GFRP) bars in seawater and sea sand concrete environment, Constr. Build. Mater. 139 (2017) 467–489.

[18] F. Yan, Z. Lin, Bond durability assessment and long-term degradation prediction for GFRP bars to fiber-reinforced concrete under saline solutions, Compos. Struct. 161 (2017) 393–406.

[19] B. Benmokrane, A. Manalo, J.-c. Bouhet, K. Mohamed, M. Robert, Effects of diameter on the durability of glass fiber – reinforced polymer bars conditioned in alkaline solution, J. Compos. Constr. 21 (5) (2017) 1–12, http://dx.doi.org/10.1061/(ASCE)CC.1943-5614.0000814.

[20] A. Manalo, G. Maranan, B. Benmokrane, P. Cousin, O. Alajarmeh, W. Ferdous, R. Liang, G. Hota, Comparative durability of GFRP composite reinforcing bars in concrete and in simulated concrete environments, Cem. Concr. Compos. 109 (2020) 103564.

[21] S. Nolan, M. Rossini, A. Nanni, Seawalls, SEACON and sustainability in the sunshine state, in: Transportation Research Board 97th Annual Meeting. Washington, DC, 2018, pp. 123–129, http://dx.doi.org/10.1039/b908937c, arXiv:arXiv:1711.00066v2.

[22] ASTM International, ASTM D1141 - Standard Practice for the Preparation of Substitute Ocean Water, Technical Report, 2013.

[23] L. Montanari, P. Suraneni, M. Tsui-Chang, M. Khatibmasjedi, U. Ebead, J. Weiss, A. Nanni, Hydration, pore solution, and porosity of cementitious pastes made with seawater, J. Mater. Civ. Eng. 31 (8) (2019) 4019154.

[24] ASTM International, ASTM D7705 - Standard Test Method for Alkali Resistance of Fiber Reinforced Polymer (FRP) Matrix Composite Bars used in Concrete Construction, Technical Report, 2012, http://dx.doi.org/10.1520/D7705.

[25] ASTM International, ASTM D7957 - Standard Specification for Solid Round Glass Fiber Reinforced Polymer Bars for Concrete Reinforcement, Technical Report, 2017, http://dx.doi.org/10.1520/D7957.

[26] Y.A. Al-Salloum, S. El-Gamal, T.H. Almusallam, S.H. Alsayed, M. Aqel, Effect of harsh environmental conditions on the tensile properties of GFRP bars, Compos. B 45 (1) (2013) 835–844, http://dx.doi.org/10.1016/j.compositesb.2012.05.004, URL: http://ac.els-cdn.com/S1359836812003290/1-s2.0-S1359836812003290-main.pdf?{_}tid=8744ff84-4ad6-11e7-9894-00000aacb35f{&}acdnat=1496767271{_}83178ef8388dbbbcfdf5834cb78ea5ba.

[27] O. Starkova, K. Aniskevich, J. Sevcenko, Long-term moisture absorption and durability of FRP pultruded rebars, in: Materials Today: Proceedings, 2020, http://dx.doi.org/10.1016/j.matpr.2019.12.154, URL: http://www.sciencedirect.com/science/article/pii/S2214785319341653.

[28] L. Pauling, General Chemistry, Dover Publications, 1988.

[29] K. Litherland, D. Oakley, B. Proctor, The use of accelerated ageing procedures to predict the long term strength of grc composites, Cem. Concr. Res. 11 (3) (1981) 455–466, http://dx.doi.org/10.1016/0008-8846(81)90117-4, URL: https://www.sciencedirect.com/science/article/pii/0008884681901174.

[30] L.C. Bank, T.R. Gentry, B.P. Thompson, J.S. Russell, A model specification for FRP composites for civil engineering structures, Constr. Build. Mater. 17 (6-7) (2003) 405–437.

[31] G. Wu, Z. Dong, X. Wang, Y. Zhu, Z. Wu, Prediction of long-term performance and durability of BFRP bars under the combined effect of sustained load and corrosive solutions, J. Compos. Constr. 19 (3) (2014) 4014058, http://dx.doi.org/10.1061/(ASCE)CC.1943-5614.0000517.

[32] O. Gonenc, Durability and Service Life Prediction of Concrete Reinforcing Materials, University of Wisconsin–Madison, 2003.

[33] A. Serbescu, M. Guadagnini, K. Pilakoutas, Mechanical characterization of basalt FRP rebars and long-term strength predictive model, J. Compos. Constr. 19 (2) (2014) 4014037.

[34] A. Weber, From national approval to an european standard—ways to a safer and wider application of FRP rebars, in: FRPRCS-11, University of Minho, Guimaraes, Portugal, 2013.

[35] C. Renaud, M.E. Greenwood, Effect of glass fibres and environments on long-term durability of GFRP composites, in: Proceedings of 9 EFUC Meeting, Wroclaw, Poland, Citeseer, 2005.

[36] International Federation for Structural Concrete (fib), Fib Bulletin 40 - FRP Reinforcement in RC Structures, Technical Report, 2007, p. 160.

[37] ACI Committee 440, ACI 440.1R - Guide for the Design and Construction of Structural Concrete Reinforced with FRP Bars, Technical Report, 2015, p. 88, http://dx.doi.org/10.1061/40753(171)158.

[38] Z. Dong, G. Wu, X.L. Zhao, Z.K. Wang, A refined prediction method for the long-term performance of BFRP bars serviced in field environments, Constr. Build. Mater. 155 (2017) 1072–1080, http://dx.doi.org/10.1016/j.conbuildmat.2017.07.154.

[39] K.K. Phani, N.R. Bose, Temperature dependence of hydrothermal ageing of CSM-laminate during water immersion, Compos. Sci. Technol. 29 (2) (1987) 79–87.

[40] K.K. Phani, N.R. Bose, Temperature dependence of hydrothermal ageing of CSM-laminate during water immersion, Compos. Sci. Technol. 29 (2) (1987) 79–87, http://dx.doi.org/10.1016/0266-3538(87)90050-9.

[41] J. Wang, H. GangaRao, R. Liang, W. Liu, Durability and prediction models of fiber-reinforced polymer composites under various environmental conditions: A critical review, J. Reinf. Plast. Compos. 35 (3) (2016) 179–211.

[42] H. Saadatmanesh, F.E. Tannous, Durability of Fiber Reinforced Plastic (FRP) Rebars and Tendons in Aggressive Environments, in: Proceedings of the International Seminar on Repair and Rehabilitation of Reinforced Concrete Structures, 1998, pp. 120–133.

[43] B. Benmokrane, V.L. Brown, A.H. Ali, K. Mohamed, C. Shield, Reconsideration of the environmental reduction factor CE for GFRP reinforcing bars in concrete structures, J. Compos. Constr. 24 (4) (2020) 6020001.